Study of the Damage-induced Anisotropy of Quasi-brittle Materials using the Component Assembling Model

JING ZHANG,[1,2,*] NAI-GANG LIANG,[1] SHOU-CHUN DENG,[1,2]
JIN-XING LIU,[1,2] XIAO-YU LIU[1] AND QIANG FU[1,2]

[1]*State Key Laboratory of Nonlinear Mechanics (LNM), Institute of Mechanics, Chinese Academy of Sciences, Beijing, 100080, China*

[2]*Graduate University of Chinese Academy of Sciences Beijing, 100080, China*

ABSTRACT: Damage-induced anisotropy of quasi-brittle materials is investigated using component assembling model in this study. Damage-induced anisotropy is one significant character of quasi-brittle materials coupled with nonlinearity and strain softening. Formulation of such complicated phenomena is a difficult problem till now. The present model is based on the component assembling concept, where constitutive equations of materials are formed by means of assembling two kinds of components' response functions. These two kinds of components, orientational and volumetric ones, are abstracted based on pair-functional potentials and the Cauchy–Born rule. Moreover, macroscopic damage of quasi-brittle materials can be reflected by stiffness changing of orientational components, which represent grouped atomic bonds along discrete directions. Simultaneously, anisotropic characters are captured by the naturally directional property of the orientational component. Initial damage surface in the axial-shear stress space is calculated and analyzed. Furthermore, the anisotropic quasi-brittle damage behaviors of concrete under uniaxial, proportional, and nonproportional combined loading are analyzed to elucidate the utility and limitations of the present damage model. The numerical results show good agreement with the experimental data and predicted results of the classical anisotropic damage models.

KEY WORDS: anisotropic damage, quasi-brittle materials, initial damage surface, uniaxial tension, non-proportional loading, component assembling model.

*Author to whom correspondence should be addressed. E-mail: zhangj@lnm.imech.ac.cn
Figures 2, 8 and 15 appear in color online: http://ijd.sagepub.com

1056-7895/08/03 0197–25 $10.00/0 DOI: 10.1177/1056789508089229

Los Angeles, London, New Delhi and Singapore

INTRODUCTION

THE DAMAGE OF most quasi-brittle materials, such as certain ceramic, concrete, or rocks has significant anisotropic characteristics generally even if these materials are originally isotropic (Kachanov, 1992; Lemaitre, 1992; Murakami and Kamiya, 1997; Skrzypek and Gancarski, 1998). For most brittle or quasi-brittle materials, the generation, nucleation, and growth of the distributed and oriented microcracks are predominant in this damage process to cause the distinct deterioration of material properties in different directions, which can be observed experimentally (Litewka, 1986; Litewka et al., 2003). This problem of damage with oriented microcracks is generally called damage-induced anisotropy or anisotropic damage. Anisotropic damage usually accompanied by nonlinearity and strain softening is a complicated and difficult problem.

Continuum damage mechanics (CDM) and microscopic damage mechanics have investigated such deteriorating phenomena from different aspects. In CDM, the damaged quasi-brittle material may be treated as a fictitious continuum with microcracks uniformly smeared within its volume. Therefore, the associated damage induced anisotropy has been modeled at the macroscopic level by means of vector damage variable (Krajcinovic and Fonseka, 1981; Singh and Digby, 1989), second-order damage tensor (Murakami and Kamiya, 1997; Halm and Dragon, 1998; Dragon et al., 2000; Litewka and Dębiński, 2003), fourth-order damage tensor (Chow and Wang, 1987; Simo and Ju, 1987; Chaboche, 1993; Chaboche et al., 1995), or even higher order damage tensor (Krajcinovic and Mastilovic, 1995). Microscopic damage mechanics aims to solve this problem by relating the microstructural state of the damaged material to its macroscopic response (Horii and Nemat-Nasser, 1983; Krajcinovic, 1989; Bažant and Planas, 1998; Basista, 2003; Pensee and Kondo, 2003). In spite of the great progress in this field, some limitations still exist in these phenomenological and micromechanical damage models. First, the formulations of most anisotropic damage models are too complex to be implemented in a practicable and efficient manner with many material parameters to be specified (Krajcinovic, 2000; Leukart and Ramm, 2003; Feng et al., 2004). Second, in most models, microcracks are assumed to have fixed directions, but they usually do not have the same orientation during damage process even if the principal stress direction remains fixed. It is still a hard problem as far as the directions of microcracks are concerned. Third, most of the previous damage models feel hard to deal with problems of complex loadings (Feng et al., 2004). Finally, with the improvements in computing technology, an anisotropic damage model is expected to be not only representing the underlying microstructures but relatively convenient in

implementation into computing programs. Hitherto, the formulation of mechanical behaviors of damaged quasi-brittle materials is still one of the actual problems of mechanics of solids (Dragon, 2002; Pensee and Kondo, 2003; Feng et al., 2004).

Based on the pair-functional potentials and the Cauchy–Born rule, Deng et al. (2006) promoted the component assembling model (CAM) to exploit the material behaviors in a relatively simple way. The total potential energy of the deformed material is calculated by 'pair-functional' potentials which are composed of pair potentials and embedding potentials. Pair potentials are grouped according to discrete directions of atomic bonds such that each group is represented by a one-dimensional orientational component. Meanwhile, a volumetric component is derived from the embedding potentials. Therefore, the material can be treated as components assembly and its constitutive equations are formed by means of assembling these two kinds of components' response functions. Thus, macroscopic behaviors of damaged material can be reflected by the stiffness changing of these orientational components. Simultaneously, the anisotropic behavior of damaged quasi-brittle materials is captured by the naturally directional property of this one-dimensional orientational component.

This article focuses on the study of the damage-induced anisotropy of quasi-brittle materials using the component assembling model. In the following section, the CAM for damage analysis is introduced from a viewpoint different from that of Deng et al. (2006) and the reason for anisotropic prediction is described. Verification of this model and the description of damage-induced anisotropy should be preceded by wide and detailed analyses. Therefore, numerical schemes for special cases are discussed. Verifications by comparisons with experiment (Gopalaratnam and Shah, 1985) and the classical anisotropic damage model promoted by Murakami and Kamiya (1997) (MK model) are investigated and discussed in detail. In the last section, a concise conclusion about the validation of the present model is given.

COMPONENT ASSEMBLING MODEL FOR DAMAGE ANALYSIS

For quasi-brittle materials, at the atomic scale, damage is the continually debonding process of atomic bonds. Whereas the damage process is the continuous evolution of microcracks at the microscopic scale, at the macroscopic scale, the damaged material shows deterioration of overall mechanical properties, as illustrated in Figure 1. As the orientation of microcracks can be observed experimentally (Litewka, 1986; Litewka et al., 2003), similarly, the fundamental process of debonding also has this

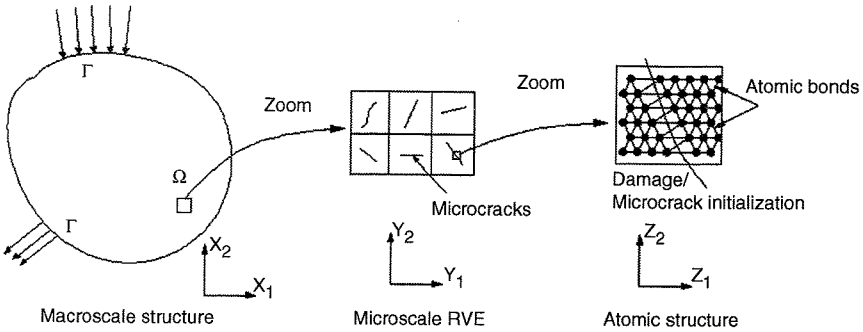

Figure 1. *Damage of quasi-brittle materials in multi-scales.*

directional character. Therefore, it is reasonable to describe damage by considering the physical and geometrical nature of the solid microstructures from the crystal lattice. This concept has been exploited in previous works (Woo and Li, 1993; Gao and Klein, 1998; Krajcinovic, 1998, 2002; Miller et al., 1998) and is investigated in CAM.

Introduction to the Component Assembling Model

Considering that the solid material is composed of a huge number of atoms, the potential energy can be approximately expressed in the form of pair-functional potentials (Phillips, 2001) in Equation (1),

$$E_{\text{exact}} \rightarrow E_{\text{tot}} = \frac{1}{2}\sum_{ij}\phi(R_{ij}) + \sum_{i}F(\rho_i). \tag{1}$$

The first term $1/2\sum_{ij}\phi(R_{ij})$ describes interatomic pair potentials representing the repulsive interactions among atomic nucleus and depends only on the atomic spacing R_{ij}. The second term $\sum_i F(\rho_i)$ is the embedding potentials describing the attractive interactions between the nucleus and electrons, which is the function of the local electron density ρ_i. When external work is applied, atoms are displaced from their previous equilibrium positions and the electronic density may vary too, so the total potential energy of this material is changed consequently. The changed total potential energy per unit volume (also known as strain energy density, U) can be calculated through the current and initial configurations of all atoms in this unit volume in the form of

$$U = \frac{1}{V}[\,E_{\text{tot}}|_{\text{def}} - E_{\text{tot}}|_{\text{ref}}\,] \tag{2}$$

where V is the current volume, and $E_{\text{tot}}|_{\text{def}}$ and $E_{\text{tot}}|_{\text{ref}}$ denote the total energy at the current and initial configurations, respectively. However, direct calculation of the changed total potentials from pair-functional potentials is a huge job to run over all pairs of interactive nuclei for pair potentials and all nuclei for embedding potentials.

The CAM (Deng et al., 2006) provides a relatively effective tool to reduce the huge degrees of freedom in this computation. Based on the Cauchy–Born rule (Phillips, 2001; Steinmann et al., 2007) assuming that the atoms in a material subject to a homogeneous deformation move according to a single mapping from the undeformed to the deformed configuration, equally distributed atoms in one direction follow the same deformation locus. Therefore, the pair potentials $1/2\sum_{ij}\phi(R_{ij})$can be reformulated alternatively: the pair potentials of thousands of interactive nuclei are grouped according to the finite directions of interatomic bonds, E_{s} denotes the total pair potentials along the direction $\boldsymbol{n}^{\text{s}}$ in unit volume, thus the changed pair potentials U_{pair} can be rewritten as the summation of strain energy density E_{s} stored at atomic bonds groups instead of computations of all pairs of interactive nuclei

$$\begin{aligned} U_{\text{pair}} &= \frac{1}{V}\left[\left(\frac{1}{2}\sum_{ij}\phi(R_{ij})\right)_{\text{def}} - \left(\frac{1}{2}\sum_{ij}\phi(R_{ij})\right)_{\text{ref}}\right] \\ &= \sum_{s=1}^{m}\frac{1}{V}\left[\left(\frac{1}{2}\sum_{ij}^{R_{ij}//\boldsymbol{n}^{\text{s}}}\phi(R_{ij})\right)_{\text{def}} - \left(\frac{1}{2}\sum_{ij}^{R_{ij}//\boldsymbol{n}^{\text{s}}}\phi(R_{ij})\right)_{\text{ref}}\right] = \sum_{s=1}^{m}E_{\text{s}}. \end{aligned} \tag{3}$$

This atomic bonds group is called orientational component. As the pair potentials along one direction have only two possibilities: increase or decrease, for orientational component, it behaves under tension or compression only. Therefore, orientational component is a typical one-dimensional component.

Based on the Cauchy–Born rule, strain of the orientational component along a specified unit direction $\boldsymbol{n}^{\text{s}}$ has kinematic relations with macroscopic strain ε_{ij} as follows:

$$\lambda^{\text{s}} = n_i^{\text{s}} n_j^{\text{s}} \varepsilon_{ij}. \tag{4}$$

The sustained stress f^{s} along this direction can be expressed by:

$$f^{\text{s}} = K^{\text{s}} \Delta\Omega^{\text{s}} \lambda^{\text{s}}. \tag{5}$$

Thus strain energy density stored in one orientational component can be expressed in the form of

$$E_{\text{s}} = \frac{1}{2} K^{\text{s}} \Delta\Omega^{\text{s}} (\lambda^{\text{s}})^2 \tag{6}$$

where $K^s\Delta\Omega^s = (1/2V)\sum_{ij}^{R_{ij}//n^s}[\phi'' R_{ij}^2 - \phi' R_{ij}]$ is the stiffness of this orientational component derived from pair-functional potentials (Deng et al., 2006), R_{ij} indicates the initial atomic bond length parallel direction $\boldsymbol{n}^s$, $\Delta\Omega^s$ is the solid angle occupied by this direction, and $K^s\Delta\Omega^s$ represents the dependency of the pair potentials to the changing of all atomic bonds' length parallel to this direction in unit volume. Thus, from Equations (3), (4), and (6), E_s can be reformulated as:

$$\begin{aligned} E_s &= \frac{1}{V}\left[\left(\frac{1}{2}\sum_{ij}^{R_{ij}//n^s}\phi(R_{ij})\right)_{\text{def}} - \left(\frac{1}{2}\sum_{ij}^{R_{ij}//n^s}\phi(R_{ij})\right)_{\text{ref}}\right] \\ &= \frac{1}{2}K^s\Delta\Omega^s(\lambda^s)^2 = \frac{1}{2}K^s\Delta\Omega^s\varepsilon_{ij}\varepsilon_{kl}n_i^s n_j^s n_k^s n_l^s. \end{aligned} \tag{7}$$

The microstructure and its evolution relating the interatomic bonds are embodied on this energy changing in orientational components. Therefore, the change of the pair potentials can be obtained by the summation of all orientational components' strain energy density,

$$U_{\text{pair}} = \sum_{s=1}^{m} E_s = \sum_{s=1}^{m}\frac{1}{2}(K^s\Delta\Omega^s)\varepsilon_{ij}\varepsilon_{kl}n_i^s n_j^s n_k^s n_l^s. \tag{8}$$

Similarly, for the embedding potentials $\sum_i F(\rho_i)$ that are dependent on the local electron density, based on the Cauchy–Born rule, their changes are related to volumetric change. Because of homogeneous deformation, the relations between the volumetric strain ε_V and the changed embedding potentials $U_{\text{embedding}}$ are set up in the form of

$$\varepsilon_V = \varepsilon_{ii} = \varepsilon_{ij}\delta_{ij} \tag{9}$$

$$U_{\text{embedding}} = \frac{1}{V}\left[\left(\sum_{i=1}F(\rho_i)\right)_{\text{def}} - \left(\sum_{i=1}F(\rho_i)\right)_{\text{ref}}\right] = \frac{1}{2}\Theta(\varepsilon_V)^2 = \frac{1}{2}\Theta\varepsilon_{ij}\varepsilon_{kl}\delta_{ij}\delta_{kl} \tag{10}$$

where $\Theta = 1/V\sum_i(F''\rho_i^2 + F'\rho_i)$ is the bulk modulus (Deng et al., 2006), representing the dependency of embedding potentials on the change of the local electron density, and δ_{ij} is the Dirac delta function. Therefore, a volumetric component is abstracted to characterize the variation of the embedding potentials. The born hydrostatic stress p of volumetric component is written as:

$$p = \Theta\varepsilon_V. \tag{11}$$

Thus the strain energy density of deformed material U is calculated from the components assembly instead of running over all pairs of interactive nuclei for pair potentials and all nuclei for embedding potentials:

$$\begin{aligned} U &= \frac{1}{V}[E_{\text{tot}}|_{\text{def}} - E_{\text{tot}}|_{\text{ref}}] = U_{\text{pair}} + U_{\text{embedding}} \\ &= \sum_{s=1}^{m} \frac{1}{2}(K^s \Delta\Omega^s) n_i^s n_j^s n_k^s n_l^s \varepsilon_{ij}\varepsilon_{kl} + \frac{1}{2}\Theta\varepsilon_{ij}\varepsilon_{kl}\delta_{ij}\delta_{kl}. \end{aligned} \tag{12}$$

Once the strain energy density of solid materials is given, the constitutive equations can be derived consequently as:

$$\sigma_{ij} = \frac{\partial U}{\partial \varepsilon_{ij}} = \sum_{s=1}^{m} (K^s \Delta\Omega^s) n_k^s n_l^s \varepsilon_{kl} n_i^s n_j^s + \Theta\delta_{kl}\varepsilon_{kl}\delta_{ij} = \sum_{s=1}^{m} f^s n_i^s n_j^s + p\delta_{ij} \tag{13}$$

$$C_{ijkl} = \frac{\partial^2 U}{\partial \varepsilon_{ij}\partial \varepsilon_{kl}} = \sum_{S=1}^{m} (K^s \Delta\Omega^s) n_i^s n_j^s n_k^s n_l^s + \Theta\delta_{kl}\delta_{ij}. \tag{14}$$

After the above discussion, the bridge between macroscopic material responses and components' behaviors are connected as shown in Figure 2. As observed in Equations (12)–(14), the strain energy density, macroscopic stress, and the constitutive equations can always be reformulated as

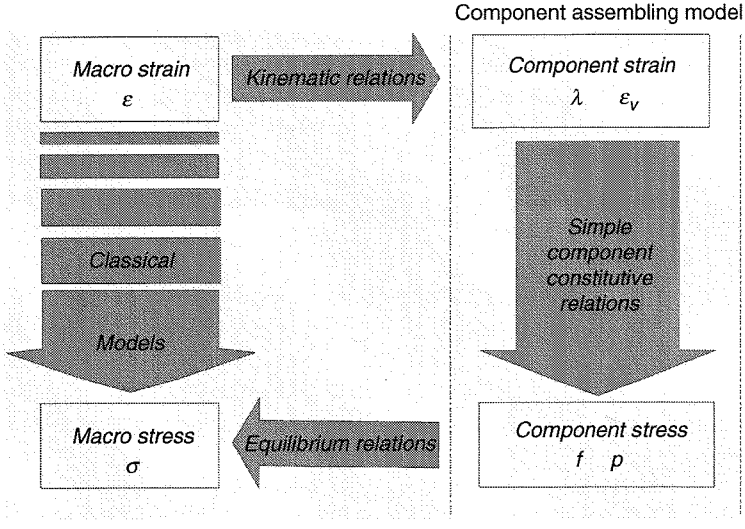

Figure 2. *Bridge between component- and macro-levels in CAM.*

the assembling of the response functions of components. These two kinds of components possess simple constitutive relations as expressed in Equations (5) and (11), but the CAM is able to put complicated mechanism into simple components' response. The key idea of the CAM that emerges is to deconstruct the complicated phenomena into simple components' response functions and reconstruct to reflect real material's behaviors by simple assembly.

For homogeneous materials, if enough orientational components spread all over the space, the summations form in Equation (14) is rewritten in the integral form,

$$\Delta\Omega = \sin\varphi d\Theta d\varphi \tag{15}$$

$$C_{ijkl} = \int_0^{\pi/2}\int_0^{\pi} K^s n_i^s n_j^s n_k^s n_l^s \sin\varphi d\varphi d\Theta + \Theta\delta_{ij}\delta_{kl}. \tag{16}$$

The integral of Equation (16) can be transformed to discrete summation for numerical computing, and the finite selected directions turn into orientational components' directions in Figure 3 as expressed in the form

$$C_{ijkl} = \sum_{s=1}^{M} K^s n_i^s n_j^s n_k^s n_l^s d\Omega^s + \Theta\delta_{ij}\delta_{kl} \tag{17}$$

where M denotes the number of finite selected directions.

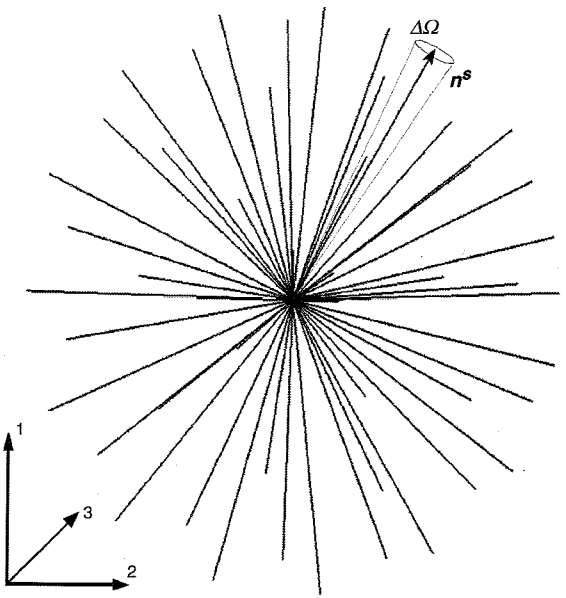

Figure 3. *3D spatial distribution of orientational components in unit hemisphere in CAM.*

For homogeneous and isotropic elastic material, the stiffness K^s for each orientational component is the same and kept constant, and the bulk modulus Θ can also be treated as a constant under small deformation. Therefore, integrating Equation (16) on the upper half of a unit sphere yields,

$$C_{ijkl} = \left(\frac{2}{15}K + \Theta\right)\delta_{ij}\delta_{kl} + \frac{2\pi}{15}K(\delta_{ik}\delta_{jl} + \delta_{il}\delta_{jk}). \tag{18}$$

Compared with traditional continuum mechanics, K and Θ are determined respectively according to the Young's modulus E and Poisson's ratio ν.

$$\begin{cases} K = \dfrac{15E}{4\pi(1+\nu)} \\ \Theta = \dfrac{(4\nu - 1)E}{2(1+\nu)(1-2\nu)} \end{cases}. \tag{19}$$

Component Assembling Model for Damage Analysis

For simplicity and exploiting the capability of the CAM primarily, the parameter Θ of volumetric component is assumed to be unchanged during the damage process. Thereby, the damage process on the orientational component only is investigated.

For quasi-brittle damage, two levels, component level and macroscopic level, are encompassed in CAM. At the component level, its stiffness K^s varies with the oriented process of atomic debonding, as the orientational component is directionally grouped atomic bonds. The more the atomic bonds are broken, the more the decrease in stiffness. Therefore, a scalar parameter D^s is introduced to represent the deterioration of orientational component as:

$$D^s = 1 - \frac{K_t^s}{K_0^s} \tag{20}$$

where K_0^s and K_t^s denote the initial and instantaneous stiffness of the orientational component, respectively. This damage variable D^s can vary in the range [0, 1]. Each orientational component has a specific damage factor D^s to characterize its current damage state. Consequently, the sustained stress f of a typical component varies according to the damage factor D^s

$$f^s = K_t^s \lambda^s = (1 - D^s)K_0^s \lambda^s. \tag{21}$$

Substituting Equation (21) into the constitutive Equation (17), one can obtain the constitutive equations for quasi-brittle damage:

$$\sigma_{ij} = \sum_{s=1}^{M} f^s n_i^s n_j^s + p\delta_{ij} = \left\{ \sum_{s=1}^{M} (1 - D^s) K_0^s n_i^s n_j^s n_k^s n_l^s + \Theta \delta_{ij} \delta_{kl} \right\} \varepsilon_{kl}. \tag{22}$$

The fourth-order stiffness tensor $\tilde{C}$ with damage can be expressed as:

$$\tilde{C}_{ijkl} = \sum_{s=1}^{M} \left\{ (1 - D^s) K_0^s n_i^s n_j^s n_k^s n_l^s \right\} + \Theta \delta_{ij} \delta_{kl}. \tag{23}$$

In order to be compared with other macroscopic damage models, at the macroscopic level, a fourth-order damage tensor $\tilde{D}$ is directly derived based on the components status to predict the deterioration of overall material properties.

$$\tilde{D}_{ijkl} = 1 - \frac{S^0_{ijkl}}{S^t_{ijkl}} = 1 - \frac{\left[(\tilde{C}^0)^{-1} \right]_{ijkl}}{\left[(\tilde{C}^t)^{-1} \right]_{ijkl}} \tag{24}$$

(i, j, k, l are not summed)

where $\boldsymbol{S}^0$ is the virgin compliance tensor and $\boldsymbol{S}^t$ is the current compliance tensor. $\boldsymbol{S}$ has the form

$$\boldsymbol{S} = \tilde{\boldsymbol{C}}^{-1}. \tag{25}$$

From Equations (23) and (24), damage-induced anisotropy is embodied because of different damage states of each orientational component. Mechanical properties in different orientations may vary for the directional property of microcracking in solid materials. Anisotropy is exactly the macroscopic response to this directional dependency. Macroscopically, damage-induced anisotropy is very complicated as far as microcracks are concerned. However, at component level in CAM, this problem is simplified substantially. In the present damage model, damage is depicted by the stiffness variation of the orientational component only. For initial homogeneous and isotropic materials, the stiffness and evolution law are the same for each orientational component. However, with respect to the load direction, each component holds different damage conditions independently in different orientations. Therefore, damage-induced anisotropy is reflected by

different damage states of orientational components during this damage process. Thus, this complicated question of oriented microcracks is simplified conveniently in the present damage model.

NUMERICAL IMPLEMENTATION

For numerical implementation of the CAM, concrete constitutive forms of the orientational component should be specified primarily. For this component, one bilinear strain–stress curve is employed in this study as shown in Figure 4. λ_c is the threshold strain for initial damage, λ_t is the ultimate strain, and its initial stiffness K_0^s is determined in Equation (19). Once component's strain λ exceeds λ_c, damage begins. As discussed before, it is admitted that every orientational component follows the same strain–stress curve for initial isotropic materials.

Case of Uniaxial Tension

In the case of the uniaxial tension analysis, for simplicity, it is assumed that the tensional and compressional characters of orientational component are the same. Therefore, only four material parameters λ_c, λ_t, E_0, and ν_0 are involved as independent variables in this damage model for uniaxial tension.

A rectangular coordinate system (x_1, x_2, x_3) is employed, where x_1 is taken as the direction of load. ε_{11}^e is positive, while ε_{22}^e and ε_{33}^e which are

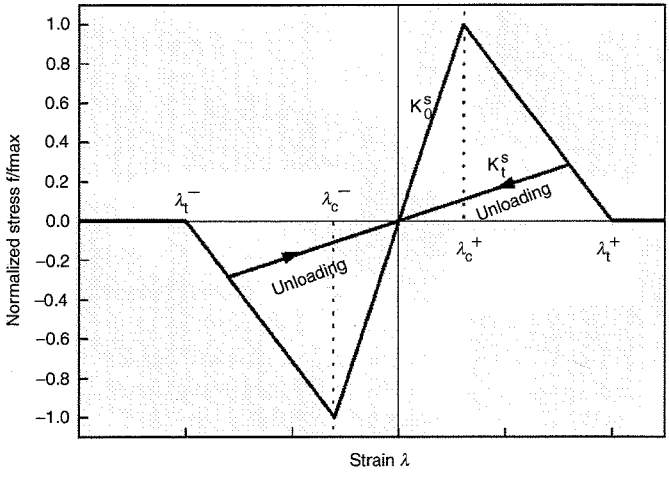

Figure 4. *Stress versus strain ($f - \lambda$) curve for the orientational component.*

perpendicular to the loading direction x_1 are negative. The elastic stress is given as:

$$[\sigma] = \begin{bmatrix} \sigma_{11} & 0 & 0 \\ 0 & 0 & 0 \\ 0 & 0 & 0 \end{bmatrix}, \quad \sigma_{11} > 0. \tag{26}$$

The state of strain has the form:

$$[\varepsilon^e] = \begin{bmatrix} \varepsilon^e_{11} & 0 & 0 \\ 0 & \varepsilon^e_{22} & 0 \\ 0 & 0 & \varepsilon^e_{33} \end{bmatrix} \tag{27}$$

The constitutive equations can be expressed as:

$$\sigma_{11} = \tilde{C}_{1111}\varepsilon^e_{11} + \tilde{C}_{1122}\varepsilon^e_{22} + \tilde{C}_{1133}\varepsilon^e_{33} \tag{28}$$

$$\sigma_{22} = \tilde{C}_{2211}\varepsilon^e_{11} + \tilde{C}_{2222}\varepsilon^e_{22} + \tilde{C}_{2233}\varepsilon^e_{33} = 0 \tag{29}$$

$$\sigma_{33} = \tilde{C}_{3311}\varepsilon^e_{11} + \tilde{C}_{3322}\varepsilon^e_{22} + \tilde{C}_{3333}\varepsilon^e_{33} = 0. \tag{30}$$

$\tilde{\boldsymbol{C}}$ is the stiffness tensor with damage as expressed in Equation (23). According to Equations (28)–(30), three unknown quantities ε^e_{11}, ε^e_{22}, and ε^e_{33} can be solved and the stiffness tensor $\tilde{\boldsymbol{C}}$ is determined simultaneously.

Therefore, the apparent Poisson's ratio $\tilde{\nu}$ can be obtained in the form

$$\tilde{\nu}_{12} = -\frac{\varepsilon^e_{22}}{\varepsilon^e_{11}} \tag{31}$$

$$\tilde{\nu}_{13} = -\frac{\varepsilon^e_{33}}{\varepsilon^e_{11}}. \tag{32}$$

Macroscopic damage tensor is defined as the variation of compliance tensor $\boldsymbol{S}$ as expressed in Equation (24). Thus, the damage variables $\tilde{D}_{1111}$, $\tilde{D}_{2222}$, $\tilde{D}_{3333}$ and the effective Young's modulus $\tilde{E}_1$ can be reformulated consequently:

$$\tilde{D}_{1111} = 1 - \frac{\left[(\tilde{\boldsymbol{C}}^0)^{-1}\right]_{1111}}{\left[(\tilde{\boldsymbol{C}}^t)^{-1}\right]_{1111}} \approx 1 - \frac{\tilde{E}_1}{E_0} \tag{33}$$

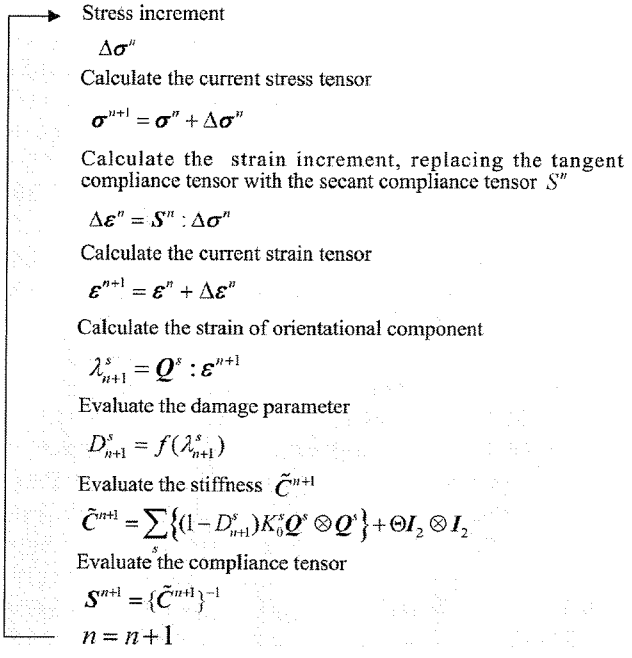

Figure 5. *Flow chart of inversion process from strain space to stress space.*

$$\tilde{D}_{2222} = 1 - \frac{\left[(\tilde{C}^0)^{-1}\right]_{2222}}{\left[(\tilde{C}^t)^{-1}\right]_{2222}} \approx 1 - \frac{\tilde{E}_2}{E_0} \tag{34}$$

$$\tilde{D}_{3333} = 1 - \frac{[(\tilde{C}^0)^{-1}]_{3333}}{[(\tilde{C}^t)^{-1}]_{3333}} \approx 1 - \frac{\tilde{E}_3}{E_0} \tag{35}$$

$$\tilde{E}_1 \approx (1 - \tilde{D}_{1111}) E_0 \tag{36}$$

where $\tilde{E}_1$ is the effective Young's modulus along the load direction and E_0 is the initial Young's modulus. Within this study, 2560 orientational components and 1 volumetric component are incorporated.

Case of Inverse Process from Strain Space to Stress Space

The present damage model is formulated in strain space. However, one needs to discuss questions in stress space in some cases, such as non-proportional loading problem. Therefore, an inverse process is needed for the present model. The detailed algorithm of implementation is listed in Figure 5, where the state at the start of a loading increment is

denoted as n and the end state as $n+1$. For given macroscopic strain $\boldsymbol{\varepsilon}^n$, corresponding compliance tensor $\boldsymbol{S}^n$ can be determined, where compliance tensor $\boldsymbol{S}^n$ is the inverse tensor of stiffness tensor $\tilde{\boldsymbol{C}}^{\mathbf{n}}$. For next iteration, $\boldsymbol{S}^{n+1}$ is assigned value of the compliance tensor $\boldsymbol{S}^n$. Thus, for a given stress increment $\Delta\boldsymbol{\sigma}^{n+1}$, corresponding strain increment $\Delta\boldsymbol{\varepsilon}^{n+1}$is approximately obtained using the compliance tensor $\boldsymbol{S}^{n+1}$. This iteration continues until the end.

NUMERICAL EXAMPLES

In this section, four numerical examples are provided to evaluate the accuracy of the present model and its ability to predict the damage-induced anisotropy. These numerical simulations include the prediction of initial damage surface, uniaxial tension, and non-proportional loading problems. The numerical results are compared with experimental data and the predicted results of the MK model, respectively.

Initial Damage Surface in Stress Plane (σ_{11}, σ_{12})

The initial damage surface can be easily obtained through orientational components' assembly where the complex six-dimensional strain–stress space is decomposed into one-dimensional component space in CAM as expressed in Equations (22) and (23). For each orientational component, it has only two conditions, tension or compression. Therefore, initial criteria for damage are promoted for tension and compression components, respectively:

$$\begin{cases} \max\{\lambda^s, s = 1, \ldots m\} = \lambda_c^+, & \text{in tension} \\ \min\{\lambda^s, s = 1, \ldots m\} = \lambda_c^-, & \text{in compression} \end{cases} \tag{37}$$

where λ_c^+ and λ_c^- are threshold values for tension and compression components, respectively. For a specific proportional loading path, once the strain of an orientational component λ^s reaches its threshold, damage begins. Therefore, initial damage surface comes into being in stress subspace after running over all proportional loading paths accordingly.

In stress subspace (σ_{11}, σ_{12}), ε_{11}, ε_{22}, ε_{33} and ε_{12} are the only four non-zero components of strain. Substituting these non-zero strain components

into Equation (4), the strain of orientational component in direction $\boldsymbol{n}^s$ can be expressed as:

$$\lambda^s = \frac{\sigma_{11}}{E}[(n_1^s)^2 - \nu(n_2^s)^2 - \nu(n_3^s)^2] + \frac{2\sigma_{12}}{E}(1+\nu)n_1^s n_2^s. \tag{38}$$

For each loading path, there is a specific corresponding direction where the strain (tension/compression) of orientational component varies fastest, that is to say, there is a specific orientational component to reach threshold value first for each loading path. Then, according to initial criteria for damage as expressed in Equation (37), initial damage surface is advantageously drawn up in stress subspace $(\sigma_{11}, \sigma_{12})$ after running over all loading paths as shown in Figure 6.

As observed in Figure 6, the predicted initial damage surface by the present model with four material parameters, $E = 21.4$ GPa, Poisson's ratio $\nu = 0.2$, $\lambda_c^+ = 0.0004$, and $\lambda_c^- = -0.001$, is consistent with the predicted results by the MK model with nine parameters. Intersecting points of initial damage surface and stress axes are the same for these two models, and initial damage surface in the first and fourth quadrants fits close. However, there exist salients in the second and third quadrants for the present model. The reason is that in the right hand of the salient, initial damage surface is controlled by components in tension, yet, in the left hand of the salient,

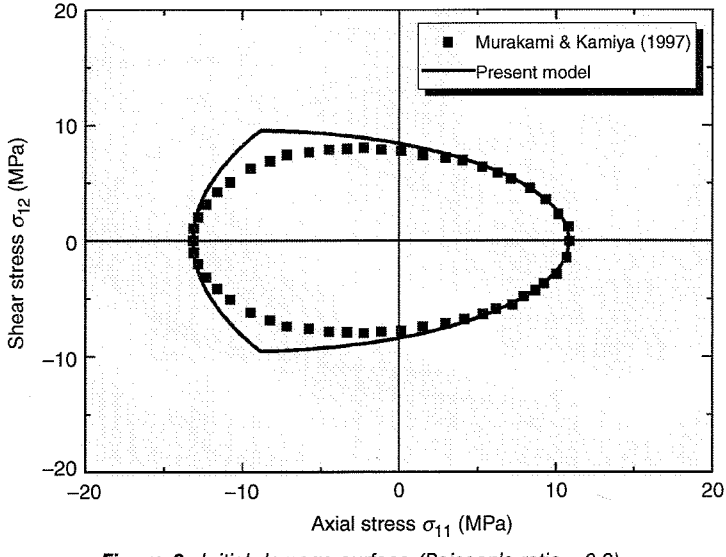

Figure 6. *Initial damage surface (Poisson's ratio = 0.2).*

damage surface is decided by components in compression. Therefore, the convex corner is formed by juncture because threshold values for tension and compression components are different.

Further investigations of initial damage surface have been performed on the effect of Poisson's ratio. Under the conditions of $\lambda_c^+ = 0.0004$, $\lambda_c^- = -0.001$, and $E = 21.4\,\text{GPa}$, 0.2, 0.3, and 0.4 are assigned to Poisson's ratio respectively. It can be seen from Figure 7 that intersecting points of damage surface and axial stress σ_{11} axis remain unchanged with the variation of Poisson's ratio. That is to say, initial damage points for uniaxial tension and uniaxial compression are independent of Poisson's ratio. However, the area enclosed by damage surface decreases with the increase of Poisson's ratio. This is mainly because the influence of the one axial loading to lateral axis increases with the Poisson's ratio. Therefore, components' strain will increase accordingly. This means the component reaches its threshold value more quickly. In this way, the area of initial damage surface will shrink with the increase of Poisson's ratio. Moreover, the salient angle becomes smooth and eventually disappears with the increment of Poisson's ratio as indicated in Figure 7. This reason can be revealed from computed results. In the case of Poisson's ratio $v = 0.3$, the convex angle moves leftwards and becomes flat because the area controlled by compression

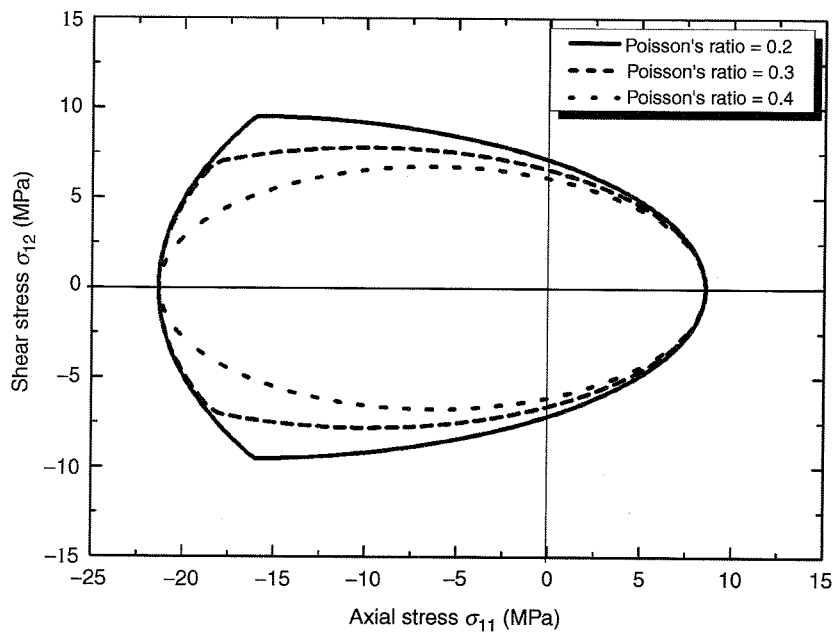

Figure 7. *Effect of the Poisson's ratio to initial damage surface.*

components is reduced. Finally, when Poisson's ratio is 0.4, the whole region of initial damage surface is controlled by tension components only, then convex angle is eliminated.

Uniaxial Tension

CASE 1: COMPARISONS WITH EXPERIMENTAL DATA

The authors confirm the validity of the present model and numerical implementation by experimental data first. In doing so, the predicted results of the present model are compared with the test results under uniaxial tension of unconfined concrete specimen, which was performed by Gopalaratnam and Shah (1985).

The material constants for the present model are determined below: $E_0 = 31.8\,\text{GPa}$, $\nu_0 = 0.18$, $\lambda_c = 0.0001$, and $\lambda_t = 0.00015$.

Numerical results are compared with experimental data as illustrated in Figure 8. There is an accurate estimate for the peak load and the pre-peak phase. However, an overestimation of material tensile strength at the first half of softening branch is observed and the stress is reduced to zero quickly. This is mainly caused by the bilinear strain–stress curve for orientational

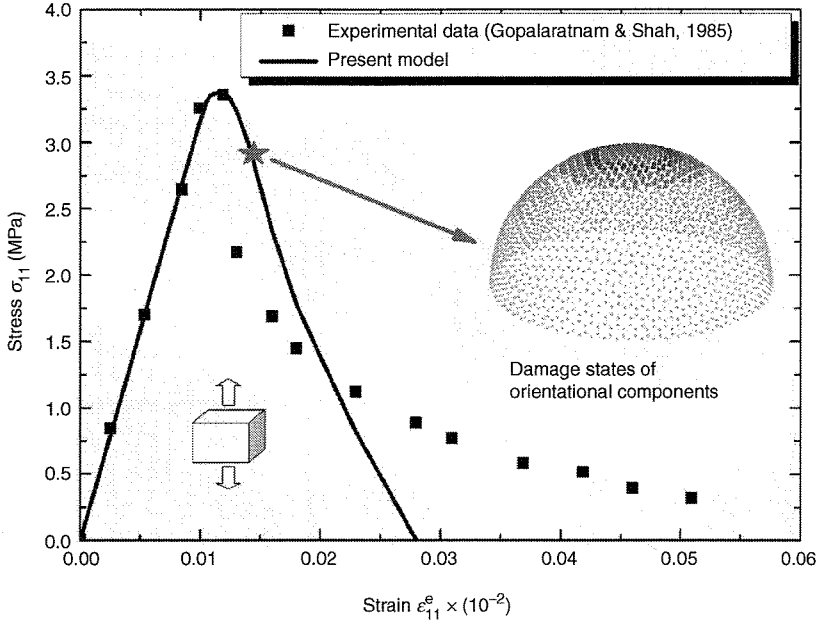

Figure 8. *Comparisons of numerical solutions against experimental results under uniaxial tension and the damage states of orientational components.*

component shown in Figure 4. It could be improved by trilinear strain–stress curve for orientational component. Under uniaxial loading, transverse isotropy is developed due to oriented microcracks' growth, which has already been observed experimentally for concrete (Litewka et al., 2003). This phenomenon of anisotropic damage growth can also be observed in the damage diagram of orientational components in Figure 8 at the right-hand side. Different colors on the hemisphere show components' different damage states. The above results confirm the validity of the present model and damage-induced anisotropy primarily. In the following cases, anisotropic behaviors will be examined preciously.

CASE 2: COMPARISON WITH MK MODEL

To further investigate the anisotropic characteristics of the present damage model, the process of elastic deformation and brittle damage of unconfined high-strength concrete are analyzed and compared with the results by MK model. In this case, four material constants, $E_0 = 21.4\,\text{GPa}$, $\nu_0 = 0.2$, $\lambda_c = 0.00045$, and $\lambda_t = 0.0020$, are employed in the present model.

The symbols and the solid line in Figure 9, respectively, show the predicted results by the MK model and the present model for the stress–strain relation of high strength concrete under uniaxial tension.

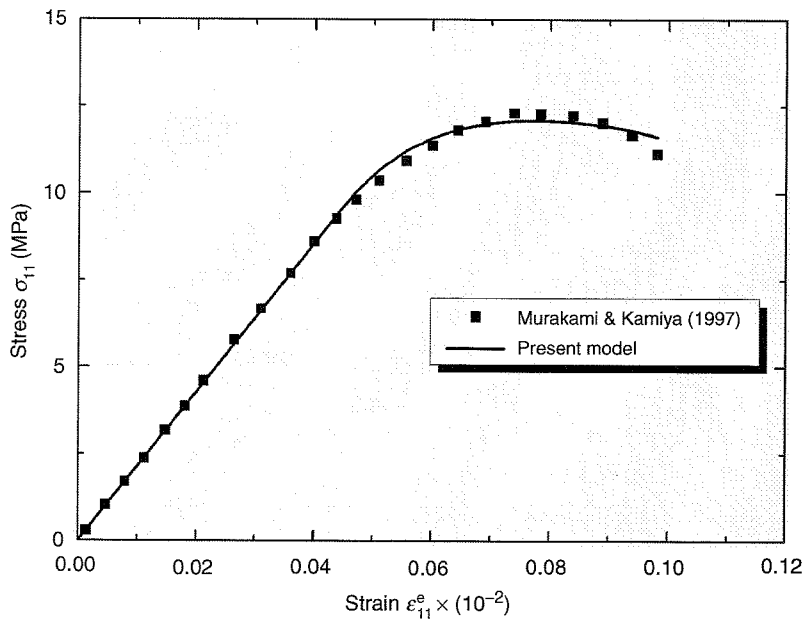

Figure 9. *Predicted results of the stress–strain relation under uniaxial tension.*

As observed in Figure 9, the results of the present model show good agreement with those predicted by the MK model.

Figures 10 and 11 are the predictions of the Young's modulus–strain relation and the apparent Poisson's ratio–strain relation of the present model compared with the results by the MK model. These results represent the characteristic features of damaged quasi-brittle materials. The decrease of the Young's modulus due to the development of damage is clearly illustrated in Figure 10. The change of apparent Poisson's ratio is one aspect of anisotropic damage characteristics where Poisson's ratio decreases as the strain grows under uniaxial tension. The results of the MK model show that Poisson's ratio decreases slowly under uniaxial tension, while in the present model, Poisson's ratio decreases rapidly which is more consistent with the predicted results of Krajcinovic and Fonseka (1981). Moreover, the apparent Poisson's ratio $\tilde{\nu}_{12} = \tilde{\nu}_{13}$ also confirms the transformation from initial isotropy to transverse isotropy under uniaxial tension.

It can be seen from Figures 12 and 13 that the damage component $\tilde{D}_{1111}$ which represents the damage along loading direction is much larger than other components $\tilde{D}_{2222}$ and $\tilde{D}_{3333}$. This result shows significant anisotropic behavior of damage under uniaxial tension. In addition, it can be observed from Figure 12 that $\tilde{D}_{1111}$ of the present model is much larger than D_{11} of

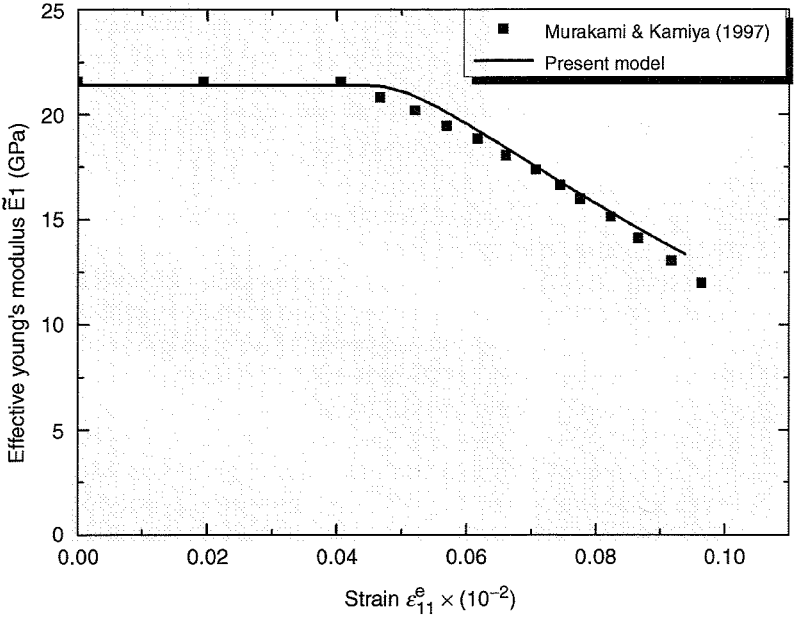

Figure 10. *Predicted results of Young's modulus under uniaxial tension.*

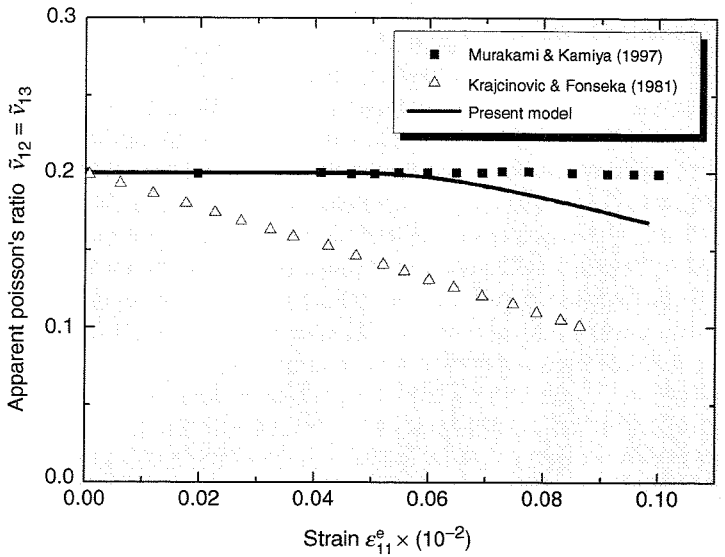

Figure 11. *Predicted results of Poisson's ratio under uniaxial tension.*

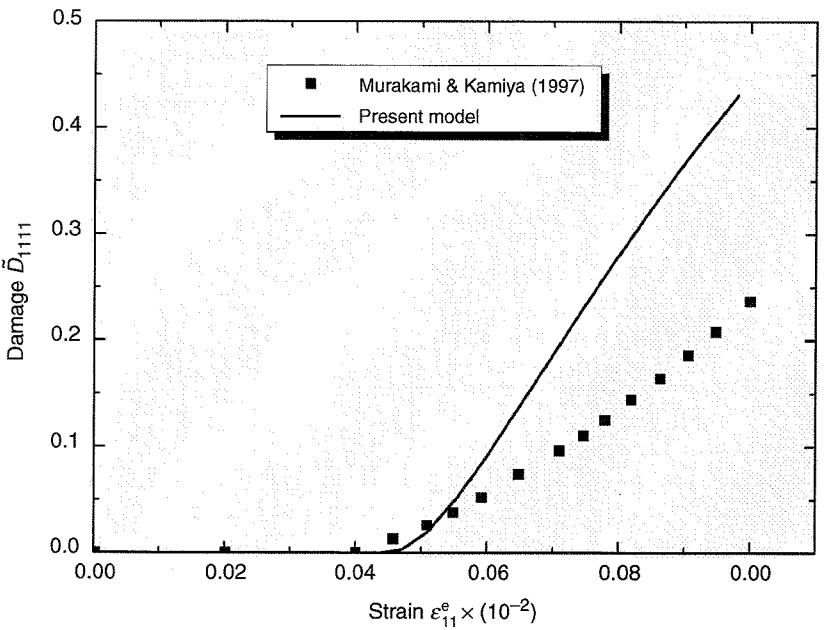

Figure 12. *Predicted results of $\tilde{D}_{1111}$ - strain relation under uniaxial tension.*

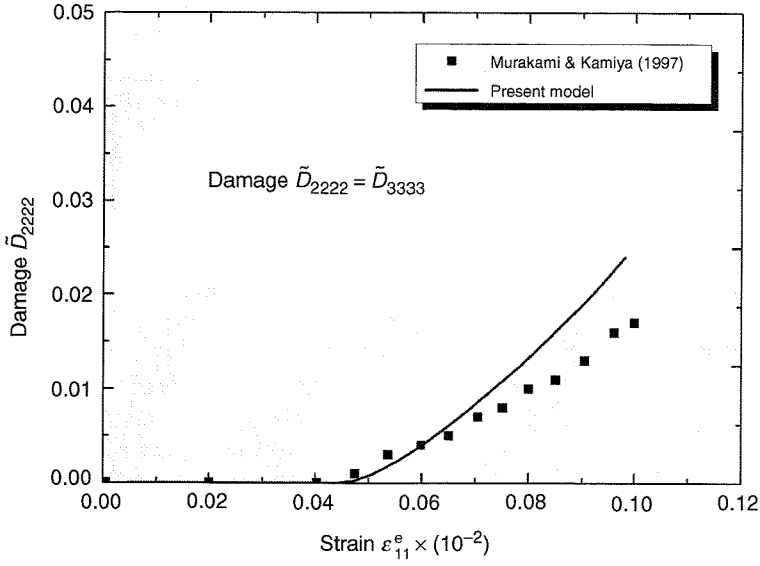

Figure 13. *Predicted results of $\tilde{D}_{2222}$-strain relation under uniaxial tension.*

the MK model. The most possible reason is that the definitions of macroscopic damage variables are different. In the MK model, damage variables represent the reduction of net area; yet, damage component $\tilde{D}_{1111}$ is defined as the reduction of stiffness in the present model, i.e., the weak nature of the Young's modulus in the load direction.

Strain Path Dependence on Quasi-brittle Materials

The calculation of non-proportional loading is a hard problem for many damage models. However, it is an important aspect of anisotropic characteristics in quasi-brittle damage. Therefore, the elastic-brittle damage responses under non-proportional stress paths are predicted, with the same four material parameters determined in the above uniaxial tension for unconfined high-strength concrete: $E_0 = 21.4$ GPa, $\nu_0 = 0.2$, $\lambda_c = 0.00045$, and $\lambda_t = 0.0020$. Only four material parameters are employed in the present model, and nine material parameters are needed in the MK model. In this example, the according strain paths are calculated from three stress paths using the inverse process and the numerical results are compared with those of the MK model.

Figure 14 shows three stress paths. Figure 15 shows the calculated three strain paths by the present model and the MK model corresponding to these stress paths. Despite that each stress path in Figure 14 leads to the same stress

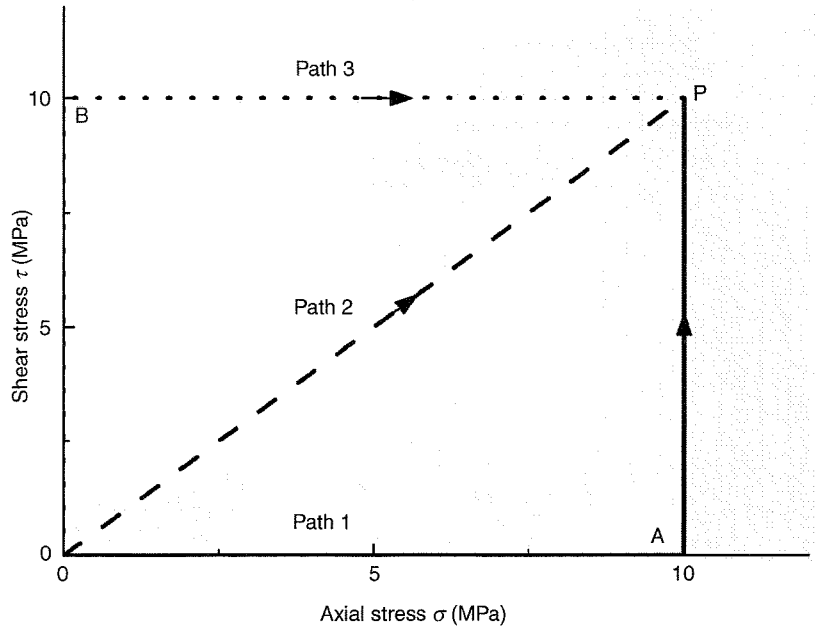

Figure 14. *Shear stress–axial stress paths.*

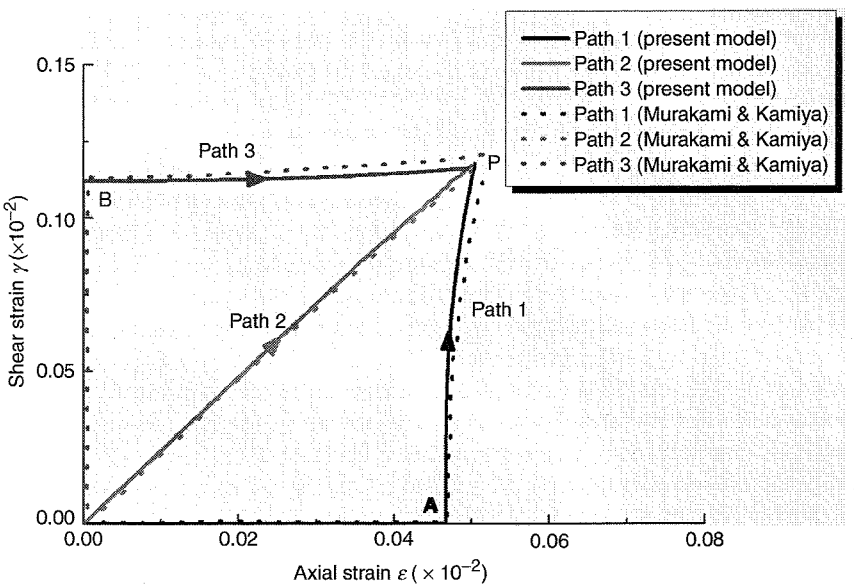

Figure 15. *Predicted results of the shear strain–axial strain paths.*

Table 1. Predicted ultimate strain points of the present model for three stress paths.

Stress path	Axial strain	Shear strain
Path 1	0.000504	0.001178
Path 2	0.000500	0.001172
Path 3	0.000495	0.001162

state P, the corresponding strain paths lead to slightly different strain states for the present model as indicated in Figure 15 and Table 1. Furthermore, each strain path shows significant non-linearity due to the different ways of development of anisotropic damage. The above features are attributable to the path dependence of the damage development (Murakami and Kamiya, 1997). It can be seen from Figure 15 that the predicted results of the present model are in very good agreement with those of the MK model. Therefore, CAM is capable of predicting anisotropic damage growth in rock-like materials, without limitation to proportional loading.

CONCLUSIONS

Anisotropic characters of damaged quasi-brittle materials are exemplified using component assembling model by the decrease of Poisson's ratio in uniaxial tension, strain path dependence in non-proportional loading, unilateral nature of initial damage surface, and so on in this study. Numerical results are compared with experimental data and those of theoretical models and show good agreement. Therefore, these numerical examples demonstrate that the present model is capable of predicting complicated anisotropic behaviors because of the naturally directional property of orientational component even though these components have very simple constitutive relations. Moreover, only four material parameters are enough to predict damage-induced anisotropy in the present model and formulations of the present model are simple, which is very important for numerical and engineering applications. Further investigations are needed to exploit the utility of the CAM, and the more general cases of bi-axial and tri-axial state of stress will be extensively investigated in future research.

ACKNOWLEDGMENTS

This research work was sponsored by National Natural Science Foundation of China through Grant No.10572140 & No. 10232050, and also partly by Ministry of Science and Technology Foundation No. 2002CB412706.

REFERENCES

Basista, M. (2003). Micromechanics of Damage in Brittle Solids, *Anisotropic Behaviour of Damaged Materials*, pp. 221–258, Berlin: Springer.

Bazănt, Z.P. and Planas, J. (1998). *Fracture and Size Effect in Concrete and Other Quasibrittle Materials*, CRC Press, Boca Raton.

Chaboche, J.L. (1993). Development of Continuum Damage Mechanics for Elastic Solids Sustaining Anisotropic and Unilateral Damage, *International Journal of Damage Mechanics*, **2**(4): 311–329.

Chaboche, J.L., Lesne, P.M. and Maire, J.F. (1995). Continuum Damage Mechanics, Anisotropy and Damage Deactivation for Brittle Materials like Concrete and Ceramic Composites, *International Journal of Damage Mechanics*, **4**(1): 5–22.

Chow, C.L. and Wang, J. (1987). An Anisotropic Theory of Continuum Damage Mechanics for Ductile Fracture, *Engineering Fracture Mechanics*, **27**(5): 547–558.

Deng, S.C., Liu, J.X., Zhang, J. and Liang, N.G. (2006). Component Assembling Model and its Application to Quasi-brittle Damage, *Theoretical and Applied Fracture Mechanics*, **46**(3): 232–242.

Dragon, A. (2002). Continuum Damage Mechanics Applied to Quasi-brittle Materials, *Continuum Damage Mechanics of Materials and Structures*, pp. 165–202, Amsterdam: Elsevier.

Dragon, A., Halm, D. and Desoyer, T. (2000). Anisotropic Damage in Quasi-brittle Solids: Modeling, Computational Issues and Applications, *Computer Methods in Applied Mechanics and Engineering*, **183**(3/4): 331–352.

Feng, X.Q., Qin, Q.H. and Yu, S.W. (2004). Quasi-micromechanical Damage Model for Brittle Solids with Interacting Microcracks, *Mechanics of Materials*, **36**(3): 261–273.

Gao, H.J. and Klein, P. (1998). Numerical Simulation of Crack Growth in an Isotropic Solid with Randomized Internal Cohesive Bonds, *Journal of Mechanics and Physics of Solids*, **46**(2): 187–218.

Gopalaratnam, V.S. and Shah, S.P. (1985). Softening Response of Plain Concrete in Direct Tension, *ACI Journal*, **82**(3): 310–323.

Halm, D. and Dragon, A. (1998). An Anisotropic Model of Damage and Frictional Sliding for Brittle Materials, *European Journal of Mechanics - A/Solids*, **17**(3): 439–460.

Horii, H. and Nemat-Nasser, S. (1983). Overall Moduli of Solids with Microcracks: Load-induced Anisotropy, *Journal of the Mechanics and Physics of Solids*, **31**(2): 155–171.

Kachanov, M. (1992). Effective Elastic Properties of Cracked Solids: Critical Review of Some Basic Concepts, *Applied Mechanics Reviews*, **45**(8): 304–335.

Krajcinovic, D. (1989). Damage Mechanics, *Mechanics of Materials*, **8**(2/3): 117–197.

Krajcinovic, D. (1998). Selection of Damage Parameter—Art or Science? *Mechanics of Materials*, **28**(1/4): 165–179.

Krajcinovic, D. (2000). Damage Mechanics: Accomplishments, Trends and Needs, *International Journal of Solids and Structures*, **37**(1/2): 267–277.

Krajcinovic, D. (2002). Essential Damage Mechanics-bridging the Scales, *Continuum Damage Mechanics of Materials and Structures*, pp. 17–47, Amsterdam: Elsevier.

Krajcinovic, D. and Fonseka, G.U. (1981). The Continuous Damage Theory of Brittle Materials Part 1: General Theory, *Journal of Applied Mechanics*, **48**(4): 809–815.

Krajcinovic, D. and Mastilovic, S. (1995). Some Fundamental Issues of Damage Mechanics, *Mechanics of Materials*, **21**(3): 217–230.

Lemaitre, J. (1992). *A Course on Damage Mechanics*, Springer-Verlag, Berlin.

Leukart, M. and Ramm, E. (2003). A Comparison of Damage Models Formulated on Different Material Scales, *Computational Materials Science*, **28**(3/4): 749–762.

Litewka, A. (1986). On Stiffness and Strength Reduction of Solids due to Crack Development, *Engineering Fracture Mechanics*, **25**(5/6): 637–643.

Litewka, A. and Dębiński, J. (2003). Load-induced Oriented Damage and Anisotropy of Rock-like Materials, *International Journal of Plasticity*, **19**(12): 2171–2191.

Litewka, A., Bogucka, J. and Dębiński, J. (2003). Anisotropic Behaviour of Damaged Concrete and Fiber Reinforced Concrete, *Anisotropic Behaviour of Damaged Materials*, pp. 185–219, Berlin: Springer.

Miller, R., Ortiz, M., Phillips, R., Shenoy, V. and Tadmor, E.B. (1998). Quasicontinuum Models of Fracture and Plasticity, *Engineering Fracture Mechanics*, **61**(3/4): 427–444.

Murakami, S. and Kamiya, K. (1997). Constitutive and Damage Evolution Equations of Elastic-brittle Materials Based on Irreversible Thermodynamics, *International Journal of Mechanics & Science*, **39**(4): 473–486.

Pensee, V. and Kondo, D. (2003). Micromechanics of Anisotropic Brittle Damage: Comparative Analysis between a Stress Based and a Strain Based Formulation, *Mechanics of Materials*, **35**(8): 747–761.

Phillips, R. (2001). *Crystals, Defects and Microstructures: Modeling Across Scales*, Cambridge: Cambridge University Press.

Skrzypek, J. and Gancarski, A. (1998). Application of the Orthotropic Damage Growth Rule to Variable Principal Directions, *International Journal of Damage Mechanics*, **7**(2): 180–206.

Simo, J.C. and Ju, J.W. (1987). Strain- and Stress-based Continuum Damage Models—I. Formulation, *International Journal of Solids and Structures*, **23**(7): 821–840.

Singh, U.K. and Digby, P.J. (1989). A Continuum Damage Model for Simulation of the Progressive Failure of Brittle Rocks, *International Journal of Solids and Structures*, **25**(6): 647–663.

Steinmann, P., Elizondo, A. and Sunyk, R. (2007). Studies of Validity of the Cauchy–Born Rule by Direct Comparison of Continuum and Atomistic Modelling, *Modelling and Simulations in Materials Science and Engineering*, **15**(1): S271–S281.

Woo, C.W. and Li, D.L. (1993). A Universal Physically Consistent Definition of Material Damage, *International Journal of Solids and Structures*, **30**(15): 2097–2108.